Journal of Sound and Vibration (1998) **211**(2), 277–291

HYBRID STRAIN-BASED THREE-NODE FLAT TRIANGULAR LAMINATED COMPOSITE SHELL ELEMENTS FOR VIBRATION ANALYSIS

C. W. S. To and B. Wang†

University of Nebraska, Department of Mechanical Engineering, 104N Walter Scott Engineering Center, Lincoln, NE 68588-0656, *U.S.A.*

(*Received* 13 *December* 1996, *and in final form* 27 *October* 1997)

1. INTRODUCTION

General surveys on dynamic analysis of composite structures were performed by Bert [1–4], Kapania and Raciti [5, 6], and Ren [7]. Several survey papers have specialized sections on this subject. For example, Reddy has reviewed finite element modelling of laminated composite plates [8] and refined theories of laminated composite plates [9]. Kapania has considered the analysis of laminated shells [10]. Yang *et al*. discussed thin shell finite elements and applications [11] while Noor and Burton examined computational models for multilayered composite shells [12].

Shear deformation theories have received considerable attention in linear vibration analysis of laminated composite structures due mainly to their advantages over classical theories. A variety of solution schemes based on first order shear deformable theory has been employed by various researchers [13–17] to solve vibration problems of laminated composite plates. References [18–20] present results of such structures by the finite element method. Examples of first order shear deformation theory used for finite element analysis of laminated composite shell structures can be found in references [21, 22]. An earlier report by Noor and Mathers [23] included shear deformation effect for a number of displacement and mixed shear–flexible finite laminated composite plate and shell elements for linear vibration problems. Applications of high order shear deformation and other theories can be found in references [12] and [24].

While shell and solid elements for modelling and analysis of layer-by-layer problems, which generally are known as local problems, have important applications in dealing with delamination, the size in term of the degrees of freedom (dof) is relatively much larger than the global problems. The main objective of the study reported in this paper is, however, concerned with global problems in which the individual layers are assumed to be perfectly bonded together. It may be appropriate to mention that the local problems are currently being studied and their results shall be reported in due course.

In this note the hybrid strain-based laminated composite three-node flat triangular shell finite elements for linear static analysis proposed by the authors [25, 26] and identified as HLCTS elements, are employed for the free vibration analysis of laminated composite plate and shell structures. The stiffness matrices of HLCTS elements have been derived and obtained explicitly in reference [26]. Thus, in the vibration analysis only the corresponding consistent element mass matrices are required. They have several important features which are different from existing similar elements. First, their derivations are obtained by using a symbolic manipulation package MACSYMA. Therefore, numerical matrix inversion and numerical integration are unnecessary in their derivations. Second, the normal rotations or so-called drilling degrees-of-freedom (ddof) are included. Third,

†Now at Quality Safety Systems Company, Tecumseh, Ontario, Canada N8N 2L9.

0022–460X/98/120277 + 15 $25.00/0/sv971373

two of these elements, with ddof based on the displacement formulation, have no shear locking, can provide the correct number of rigid body modes, and have sufficient rank and have no zero energy mode.

This note consists of five sections. The present section is an introduction whereas the following section presents the derivation of consistent element mass matrices. The third and fourth sections are concerned with numerical studies of free vibration problems of multi-layer plates and multi-layer shells, respectively. The last section includes concluding remarks.

2. ELEMENT STIFFNESS AND CONSISTENT MASS MATRICES

The formulation and derivation of the element stiffness matrices have been presented in references [26] and therefore are not included here for brevity.

The same shape functions or displacement interpolation functions adopted in the derivation of element stiffness matrices are employed. The same co-ordinate systems and two groups of displacement interpolation functions used in reference [26] are also adopted here.

The consistent element mass matrix for isotropic material is given as

$$[\mathbf{m}] = \int_V \rho[\boldsymbol{\phi}]^{\mathrm{T}}[\boldsymbol{\phi}]\,\mathrm{d}V, \tag{1}$$

where ρ is the density and $[\boldsymbol{\phi}]$ is the 18×6 displacement shape function matrix. For an element having only translational dof, equation (1) can be applied directly. For elements having translational dof, rotational dof and ddof, Liu and To [27] recommended the following consistent element mass matrix:

$$[\mathbf{m}] = \int_V [\boldsymbol{\phi}]^{\mathrm{T}}[\boldsymbol{\rho}]\,[\boldsymbol{\phi}]\,\mathrm{d}V, \tag{2}$$

where

$$[\boldsymbol{\rho}] = \begin{bmatrix} \rho & 0 & 0 & 0 & 0 & 0 \\ 0 & \rho & 0 & 0 & 0 & 0 \\ 0 & 0 & \rho & 0 & 0 & 0 \\ 0 & 0 & 0 & \rho h^2/12 & 0 & 0 \\ 0 & 0 & 0 & 0 & \rho h^2/12 & 0 \\ 0 & 0 & 0 & 0 & 0 & J \end{bmatrix}_{6\times 6}, \tag{3}$$

in which

$$J = \rho(r_2^2 + s_3^2 + r_3\,(r_3 - r_2))/18. \tag{4}$$

Equation (3) defines the generalized density matrix. It may be noted that the polar moment of inertia term, J, defined in equation (4) is specifically for the three-node flat triangular element with the chosen local co-ordinates.

For the laminated composite HLCTS elements, analogy to equation (2) is drawn and the consistent element mass matrix is defined as

$$[\mathbf{m}_e] = \sum_{k=1}^{n} \int_a [\boldsymbol{\phi}]^{\mathrm{T}} [\boldsymbol{\rho}]_k [\boldsymbol{\phi}] \, \mathrm{d}a, \tag{5}$$

where n is the total number of layers and the density matrix for the kth layer is

$$[\boldsymbol{\rho}]_k = \begin{bmatrix} \rho_k (h_k - h_{k-1}) & 0 & 0 & 0 & 0 & 0 \\ 0 & \rho_k (h_k - h_{k-1}) & 0 & 0 & 0 & 0 \\ 0 & 0 & \rho_k (h_k - h_{k-1}) & 0 & 0 & 0 \\ 0 & 0 & 0 & I_r & 0 & 0 \\ 0 & 0 & 0 & 0 & I_s & 0 \\ 0 & 0 & 0 & 0 & 0 & J_d \end{bmatrix}_{6 \times 6}, \tag{6}$$

and

$$I_r = I_s = \rho_k (h_k^3 - h_{k-1}^3)/3, \qquad J_d = \rho_k (h_k - h_{k-1}) (r_2^2 + s_3^2 + r_3 (r_3 - r_2))/18. \tag{7a, b}$$

In equations (6) and (7a, b), h_k is the layer co-ordinate in the transverse direction at the top of the kth layer (see Figure 1).

The element mass matrix defined in equation (5) is in the local co-ordinate system shown in Figure 1. Before assembling the mass matrices, they are transferred to the global co-ordinate system. The consistent element mass matrix in the global co-ordinate system is then

$$[\mathbf{M}_e] = [\mathbf{T}]^{\mathrm{T}} [\mathbf{m}_e] [\mathbf{T}], \tag{8}$$

where the transformation matrix $\mathbf{T}$ is defined in reference [26].

Applying the mass matrices derived in this section and the stiffness matrices obtained in reference [26], one can obtain six elements for vibration analysis of laminated composite plate and shell structures. These elements are denoted by $\mathrm{HLCTS}_{\mathrm{r}}^{\mathrm{qd}}$, $\mathrm{HLCTS}_{\mathrm{r}}^{\mathrm{ld}}$, $\mathrm{HLCTS}_{\mathrm{r}}^{\mathrm{qh}}$, $\mathrm{HLCTS}_{\mathrm{r}}^{\mathrm{lh}}$, $\mathrm{HLCTS}_{\mathrm{t}}^{\mathrm{qd}}$ and $\mathrm{HLCTS}_{\mathrm{t}}^{\mathrm{qh}}$, where the superscripts q, l, d and h denote, respectively, the quadratic interpolation function for transversal displacement, the linear interpolation function for transversal displacement, the displacement formulation for the

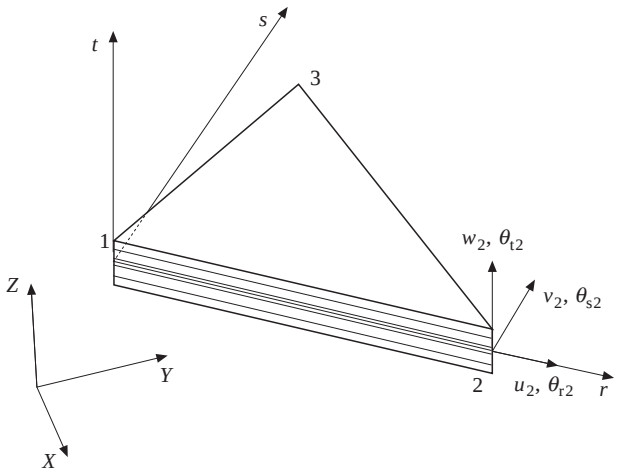

Figure 1. The three-node triangular composite laminated shell element.

ddof, and the hybrid formulation for the ddof. The subscript r refers to the case in which, in addition to the translational dof the moment of inertia and polar moment of inertia are considered, while the subscript t means that only the mass corresponding to the translational dof has been considered.

The above consistent element mass matrices have been derived and obtained explicitly by using the computer algebra package MACSYMA. For brevity, the explicit element mass matrices are not included here. It may be suffice to note that there are about 600 statements or lines in the fortran subroutines that described the above element mass matrices.

When the above HLCTS elements are employed for the vibration analysis of single layer plate and shell structures of isotropic materials, the $\text{HLCTS}_{\text{r}}^{\text{qd}}$ element, for example, reduces to that of formulation number 16 proposed by Liu and To [27].

3. VIBRATION ANALYSIS OF MULTI-LAYER PLATES

Before presenting the details of the free vibration analysis for different multi-layer cases, it should be mentioned that single element of single layer tests have been conducted to detect rigid-body modes and zero energy modes. In the tests, all the eighteen element dof are not constrained. The following remarks are in order. First, the $\text{HLCTS}_{\text{r}}^{\text{qd}}$, $\text{HLCTS}_{\text{r}}^{\text{ld}}$ and $\text{HLCTS}_{\text{t}}^{\text{qd}}$ elements have six rigid-body modes and have no zero energy modes. Second, the $\text{HLCTS}_{\text{r}}^{\text{qh}}$, $\text{HLCTS}_{\text{r}}^{\text{lh}}$ and $\text{HLCTS}_{\text{t}}^{\text{qh}}$ elements have six rigid-body modes and two zero energy modes. Third, the so-called basic triangular (BT) elements, that were presented in reference [26] and designated as BT^{q} and BT^{l} where the superscripts q and l have already been defined above, have six rigid-body modes and three zero energy modes. The zero energy modes are all associated with the in-plane torsional rotations. In other words, in the static analysis reported in reference [26] the BT elements have three zero energy modes, the HLCTS^{qh} and HLCTS^{lh} elements have two zero energy modes, and the HLCTS^{qd} and HLCTS^{ld} elements do not have any zero energy modes. In short, the displacement formulation for the ddof eliminated the spurious modes from the elements.

In addition to the above tests, a relatively comprehensive vibration analysis of single layer plates was performed. For brevity, the results of single layer cases are not included in this paper.

In this section a nine layers cross-ply symmetrically laminated square plate, and an eight layers antisymmetric laminated angle-ply square plate with different side–length ratios and length to thickness ratios are studied. Other examples have been investigated but not included here for brevity. Comparisons are made with analytical solution or other finite element solutions that are available in the literature. In the analysis the two in-plane dof, U and V (henceforth upper case refers to the global co-ordinate system), and the ddof of the HLCTS elements are constrained. The remaining dof for the HLCTS elements are associated with the bending part, that is, the transversal displacement W and two rotational dof, Θ_x and Θ_y. Therefore, only the $\text{HLCTS}_{\text{r}}^{\text{qd}}$, $\text{HLCTS}_{\text{r}}^{\text{ld}}$ and $\text{HLCTS}_{\text{t}}^{\text{qd}}$ elements are used in the investigation.

3.1. *Nine-layered cross-ply plate*

A nine-layered, cross-ply symmetrically laminated square plate with fibre orientation (0/90/0/90/0/90/0/90/0) is considered in this subsection. The side length, b, of the plate is 1·0 m (39·37 in). The total thickness of the 0° and 90° layers is the same. The thickness of the laminate is $h = 0{\cdot}01$ m (0·3937 in). The material is the high modulus graphite/epoxy composite with $E_1/E_2 = 40$, $G_{12}/E_2 = 0{\cdot}6$ and $G_{13}/E_2 = G_{23}/E_2 = 0{\cdot}5$, in which

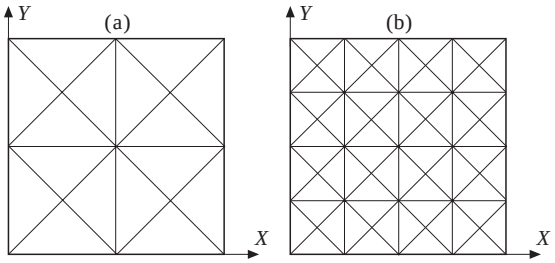

Figure 2. The square plate with D meshes: (a) 2 × 2 D mesh, (b) 4 × 4 D mesh.

$E_1 = 2{\cdot}0685 \times 10^{11}$ N/m^2 ($3{\cdot}0 \times 10^7$ psi), $\rho = 1605$ kg/m^3 ($0{\cdot}058$ lb/in^3) and Poisson's ratio $v_{12} = 0{\cdot}25$.

In this first case, the plate is simply supported at four sides (S4). It is modelled by the four finite element meshes shown in Figure 2. The shear correction factors are $\kappa_4 = \kappa_5 = (5/6)^{1/2}$. The boundary conditions are: $W = 0{\cdot}0$ at all simply supported edges, $\Theta_x = 0{\cdot}0$ at the edges parallel to Y-axis and $\Theta_y = 0{\cdot}0$ at the edges parallel to X-axis. All dof at four corners of the plate are constrained. Only the first three natural frequencies are presented in Table 1, though higher natural frequencies and mode shapes for this case and all the examples considered in this paper were obtained. They are not included here for brevity. For comparison with results in the literature, the dimensionless frequency parameter is defined as

$$\Omega = 2\pi f b(\rho/E_2)^{1/2} \times 10, \tag{9}$$

where f is the natural frequency in Hz.

TABLE 1

First three dimensionless natural frequencies of the nine-layered cross-ply S4 *plate*

		Mode sequence		
Mesh	Neq.†	1	2	3
$HLCTS_r^{qd}$				
2 × 2 D	19	2·08427	6·48111	6·83126
4 × 4 D	87	1·92484	5·55288	6·00242
6 × 6 D	203	1·89712	5·25759	5·70811
8 × 8 D	367	1·88774	5·17046	5·62086
$HLCTS_r^{ld}$				
2 × 2 D	19	2·62976	13·29262	13·92842
4 × 4 D	87	2·02886	6·35132	6·00242
6 × 6 D	203	1·94123	5·56773	5·70811
8 × 8 D	367	1·91216	5·33761	5·62086
$HLCTS_t^{qd}$				
2 × 2 D	19	2·08444	6·48249	6·83270
4 × 4 D	87	1·92500	5·55397	6·00359
6 × 6 D	203	1·89728	5·25862	5·70922
8 × 8 D	367	1·88790	5·17147	5·62195
Analytical Ref. [23]	–	1.88576	–	–

†Neg denotes the number of unknowns on dof in the solution.

TABLE 2

Comparison of the convergence on the dimensionless fundamental natural frequency of the nine-layered cross-ply S4 *plate by using different finite elements*

	Mesh (quarter plate)			
Source	2 × 2	3 × 3	4 × 4	5 × 5
SQ4	–	–	4·232	3·558
ST6	2·010	1·939	1·910	–
SQ8	1·932	1·899	1·891	1·888
SQ9	1·921	1·898	1·891	–
SQ11	1·905	1·891	–	–
ST10	1·892	1·887	–	–
SQ12	1·896	1·887	–	–
SQH	1·886	–	–	–
MT3	1·836	1·879	1·884	–
MQ4	1·877	1·884	1·885	–
MT6	1·887	–	–	–
$HLCTS_r^{qd}$	1·925	1·897	1·888	–
Analytical [23]	1·88576			

The analytical solution for the first mode in Table 1 is taken from reference [23] in which shear deformation was considered. To the best knowledge of the authors, there is no analytical solution available for the second and third modes. For the 2 × 2 D, 4 × 4 D, 6 × 6 D and 8 × 8 D meshes, the $HLCTS_r^{qd}$ results for the first mode differ from the analytical one by 10·5%, 2·1%, 0·6% and 0·1%, respectively. The corresponding discrepancies given by $HLCTS_r^{ld}$ results are 39·5%, 7·6%, 2·9% and 1·4%. It shows consistently that the $HLCTS_r^{qd}$ element has a better performance than the $HLCTS_r^{ld}$ element and therefore results for other examples using the $HLCTS_r^{ld}$ element are not included. To compare the $HLCTS_r^{qd}$ element with other finite elements in the literature, the numerical results for the same problem obtained by different finite element models are included in Table 2. The other finite element results are taken from reference [23]. In the latter the elements are all shear-deformable type and vary in formulation, element shape, and approximation of the displacement field. These features are outlined in Table 3 for convenient reference. The results in Table 2 show the convergence trend of each element. The $HLCTS_r^{qd}$ element is the simplest element listed in the table. Although it is difficult to make direct comparison when the element shape and number of nodes are different, the accuracy and efficiency can be compared when the total number of dof of a finite element model is taken into consideration. It seems that the $HLCTS_r^{qd}$ element results converge faster than the ST6 (displacement type, triangular, 6 nodes, 18 dof per element), MT3 (mixed type, triangular, 3 nodes, 24 dof per element), SQ4 (displacement type, quadrilateral, 4 nodes, 12 dof per node), SQ8 (displacement type, quadrilateral, 8 nodes, 24 dof per element), SQ9 (displacement type, quadrilateral, 9 nodes, 27 dof per element) and comparable to all the remaining elements including high-order elements, such as ST10 (displacement type, triangular, 10 nodes, 30 dof per element). For example, the MT6 element case has 200 dof with a 2 × 2 mesh and prior to the application of boundary conditions while the $HLCTS_r^{qd}$ element model has only 123 dof with a 4 × 4 D mesh, and yet their results are in excellent agreement.

TABLE 3

Description of characteristics of the shear–flexible finite elements listed in Table 2

Element	Formulation	Element shape	Approximation	Number of nodes	Total dof (for plate)
SQ4	displacement	quadrilateral	bilinear	4	12
ST6	displacement	triangular	quadratic	6	18
SQ8	displacement	quadrilateral	quadratic	8	24
SQ9	displacement	quadrilateral	quadratic	9	27
SQ11	displacement	quadrilateral	quadratic	11	33
ST10	displacement	triangular	cubic	10	30
SQ12	displacement	quadrilateral	cubic	12	36
SQH	displacement	quadrilateral	product of first order Hermitian polynomials	4	48
MT3	mixed	triangular	linear	3	24
MQ4	mixed	quadrilateral	bilinear	4	32
MT6	mixed	triangular	quadratic	6	48
$HLCTS_r^{qd}$	hybrid	triangular	quadratic for transversal displacement, linear for rotations	3	9

The nine layers cross-ply laminated square plate is then analyzed with the fully clamped (C4) and cantilevered (CFFF) boundary conditions. The clamped boundary conditions are imposed by constraining all the dof at the four sides of the plate. For the cantilevered case only one side of the square plate is clamped while the W, Θ_x and Θ_y dof of the other three edges are left free. The results are presented in Tables 4 and 5, respectively. There is no analytical or finite element solution for comparison in the C4 and CFFF cases. In Table 4, the dimensionless frequency parameters are defined by equation (9) whereas those in Table 5 are given as

$$\Omega = 2\pi f b\left(\frac{\rho}{E_2}\right)^{1/2} \times 100. \tag{10}$$

TABLE 4

First three dimensionless natural frequencies of the nine-layered cross-ply C4 *plate*

Mesh	Neq.	Mode sequence 1	2	3
$HLCTS_r^{qd}$				
2 × 2 D	15	17·0777	27·8824	27·9487
4 × 4 D	75	4·5920	10·2280	10·8644
6 × 6 D	183	4·2712	8·7165	9·3168
8 × 8 D	339	4·1768	8·3357	8·9238
$HLCTS_t^{qd}$				
2 × 2 D	15	17·0783	27·8860	27·9522
4 × 4 D	75	4·5925	10·2304	10·8670
6 × 6 D	183	4·2716	8·7184	9·3189
8 × 8 D	339	4·1772	8·3375	8·9257

TABLE 5

First three dimensionless natural frequencies of the nine-layered cross-ply cantilever plate

Mesh	Neq.	Mode sequence 1	2	3
$HLCTS_r^{qd}$				
2×2 D	30	4·5147	6·6778	37·7556
4×4 D	108	4·3719	5·7041	28·6511
6×6 D	234	4·3497	5·5261	27·4863
8×8 D	408	4·3432	5·4701	27·1613
$HLCTS_t^{qd}$				
2×2 D	30	4·5148	6·6782	37·7644
4×4 D	108	4·3720	5·7045	28·6551
6×6 D	234	4·3497	5·5265	27·4900
8×8 D	408	4·3434	5·4704	27·1649

3.2. *Eight-layered angle-ply plate*

This plate is antisymmetrically laminated with a 45° angle and stacking sequence, $(45/-45/45/-45/45/-45/45/-45)$. The side length of the plate is $b = 1{\cdot}0$ m and the thickness is $h = 0{\cdot}01$ m. The thickness of each layer is $0{\cdot}01/8$ m. The material properties are $E_1/E_2 = 40$, $G_{12}/E_2 = G_{13}/E_2 = 0{\cdot}6$ and $G_{23}/E_2 = 0{\cdot}5$, in which $E_1 = 2{\cdot}0685 \times 10^{11}$ N/m^2 ($3{\cdot}0 \times 10^7$ psi), $\rho = 1605$ kg/m^3 ($0{\cdot}058$ lb/in^3) and Poisson's ratio $\nu_{12} = 0{\cdot}25$. The plate is simply supported at four sides. The entire plate is considered in the finite element analysis. The boundary conditions imposed on the finite element models are the same as for previous S4 plate. The shear correction factors are $\kappa_4 = \kappa_5 = (\pi^2/12)^{1/2}$.

Results by using HLCTS elements are reported in Table 6. The first three natural frequencies are given as dimensionless frequency parameters defined by

TABLE 6

First three dimensionless natural frequencies of the simply supported eight-layered angle-ply square plate

Mesh	Neq.	Mode sequence 1	2	3
$HLCTS_r^{qd}$				
2×2 D	19	28·382	73·097	73·097
4×4 D	87	26·235	62·500	62·500
6×6 D	203	25·875	59·690	59·690
8×8 D	367	25·758	58·848	58·848
$HLCTS_t^{qd}$				
2×2 D	19	28·385	73·113	73·113
4×4 D	87	26·237	62·512	62·512
6×6 D	203	25·877	59·702	59·702
8×8 D	367	25·760	58·859	58·859
Analytical [28]				
FSDPT	–	25·176	–	–
HSDPT	–	25·174	–	–

$$\Omega = 2\pi f\,(b^2/h)\,(\rho/E_2)^{1/2}. \tag{11}$$

This problem has been solved by Reddy and Phan in reference [28] by applying first order shear deformation plate theory (FSDPT) and high order shear deformation plate theory (HSDPT). The available results are included in the table for comparison. For the 2×2 D, 4×4 D, 6×6 D and 8×8 D meshes, the $\text{HLCTS}_{\text{r}}^{\text{qd}}$ results of the first mode differ from the FSDPT solution by 12·7%, 4·2%, 2·8% and 2·3%, respectively.

4. VIBRATION ANALYSIS OF MULTI-LAYER SHELLS

In this stage of the investigation single-layer isotropic shell structures were studied by using the proposed finite elements. However, for brevity they are not included here. In this section, results of free vibration analysis of laminated composite shell structures are presented. A two-layered antisymmetric angle-ply laminated cylindrical panel, a four-layered symmetric cross-ply laminated cylindrical panel and a nine-layered symmetric cross-ply laminated spherical shell segment having double curvatures are included. The results, by using HLCTS elements, are compared with the existing solutions in the literature.

4.1. *Multi-layer cylindrical shells*

The first case considered in this subsection is a two-layered antisymmetric, angle-ply cylindrical shell panel. The shell panel is constructed using two equal thickness layers with fibre orientation of $(60/-60)$. The quantities in the bracket are in degrees and measured from the positive direction of the X-axis (see Figure 3). The cylindrical shell panel has a square projection plan with side length $L = 1{\cdot}0$ m. The total thickness of the shell is $h = 0{\cdot}05$ m. The radius is $R = 2{\cdot}8794$ m and the open angle is $2\varphi = 20^\circ$. The radius to side length ratio $R/L = 2{\cdot}8794$ and the side length to thickness ratio $b/h = 20$. The material used is graphite/epoxy composite with the moduli ratios: $E_1/E_2 = 40$, $G_{12}/E_2 = G_{13}/E_2 = 0{\cdot}6$, $G_{23}/E_2 = 0{\cdot}5$. The other pertinent material properties are $E_1 = 2{\cdot}0685 \times 10^{11}$ N/m^2 ($3{\cdot}0 \times 10^7$ psi), $\rho = 1605$ kg/m^3 ($0{\cdot}058$ lb/in^3) and $\nu_{12} = 0{\cdot}25$.

The cylindrical shell panel is simply supported. However, U or V perpendicular to the boundary edges are also constrained. Symmetry conditions are applied such that only one quarter of the shell is analyzed. The details of the constraints are: $V = W = \Theta_y = 0{\cdot}0$ at curve AB, $U = W = \Theta_x = 0{\cdot}0$ at straight edge BC, $V = \Theta_x = \Theta_z = 0{\cdot}0$ at curved symmetry line CD and $U = \Theta_y = \Theta_z = 0{\cdot}0$ at straight symmetry line AD. For the four corners, V and Θ_x are free at point A. All dof are constrained at point B. U and Θ_y are free at point C. The transversal deformation W is free at D. With this set of boundary conditions imposed, one can solve for doubly symmetrical modes of the simply supported multi-layer cylindrical shell panel. The shear correction factors are $\kappa_4 = \kappa_5 = (\pi^2/12)^{1/2}$.

Table 7 contains results of 2×2 D and 4×4 D mesh using the HLCTS elements. It also contains the analytical result from reference [29]. The latter gave the dimensionless frequency parameter of the first mode as 18·80. The dimensionless frequency parameter is defined by equation (11) in which b is replaced with L. In the analysis, the 4×4 D mesh results differ from the analytical solution by no more than 2·24%.

The second laminated cylindrical shell panel considered is a four-layered symmetric cross-ply cylindrical shell panel (see Figure 3). The shell is constructed of four layers with the fibre orientation in 0 and 90° directions (0/90/90/0). The geometrical properties of the panel are: $R = 1{\cdot}270$ m (50 in), $L = 0{\cdot}254$ m (10 in), $h = 0{\cdot}00254$ m ($0{\cdot}1$ in). Thus, one has $R/L = 5$ and $L/h = 100$. The layer material properties are $E_1 = 5{\cdot}1713 \times 10^{10}$ N/m^2

TABLE 7

First three dimensionless natural frequencies for the doubly symmetric modes of the simply supported two-layered angle-ply cylindrical shell panel

Source	Neq.	Mode sequence 1	2	3
2 × 2 D				
$HLCTS_r^{qd}$	45	21·167	66·668	79·451
$HLCTS_t^{qd}$	45	21·199	66·975	79·651
$HLCTS_r^{qh}$	45	21·144	66·510	79·414
$HLCTS_t^{qh}$	45	21·176	66·820	79·619
4 × 4 D				
$HLCTS_r^{qd}$	189	19·214	51·173	68·417
$HLCTS_t^{qd}$	189	19·244	51·464	68·621
$HLCTS_r^{qh}$	189	19·200	51·150	68·361
$HLCTS_t^{qh}$	189	19·230	51·441	68·566
Ref. [29]	–	18·800	–	–

($7{\cdot}5 \times 10^6$ psi), $\rho = 27\,680$ kg/m^3 ($1{\cdot}0$ lb/in^3) and $\nu_{12} = 0{\cdot}25$. The modulus ratios are $E_1/E_2 = 25$, $G_{12}/E_2 = G_{13}/E_2 = 0{\cdot}5$, $G_{23}/E_2 = 0{\cdot}2$. This cylindrical shell panel is simply supported on four sides. One quarter of the shell is solved in the current study. The boundary conditions imposed are the same as those specified in the first case above. The shear correction factors are unity. The HLCTS element results with 2 × 2 D and 4 × 4 D meshes are presented in Table 8. The results are given as dimensionless frequency parameters defined in equation (11) where b is replaced with L. The analytical solution for the first mode of this problem reported in reference [30] is 20·360. This Navier-type solution was obtained based on higher order shear deformation theory. The HLCTS element results in Table 8 are excellent. The results of the first mode for the case with 4 × 4 D mesh indicated that they are slightly below the analytical counterpart. This observation is not uncommon in elements based on mixed or hybrid formulation.

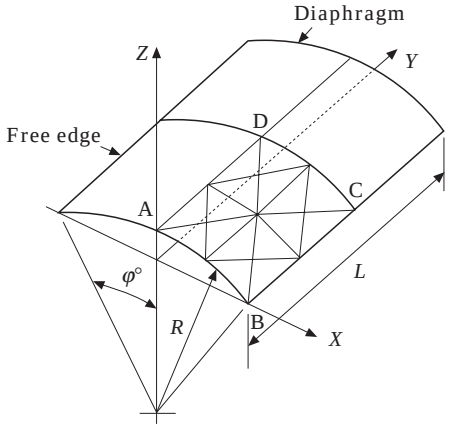

Figure 3. The Scordelis–Lo roof with 2 × 2 D mesh for one quarter of the shell.

TABLE 8

First three dimensionless natural frequencies for the doubly symmetric modes of the simply supported four-layered cross-ply cylindrical shell panel

Source	Neq.	Mode sequence 1	2	3
2 × 2 D				
$HLCTS_r^{qd}$	47	21·184	92·300	116·498
$HLCTS_t^{qd}$	47	21·186	92·350	116·546
$HLCTS_r^{qh}$	47	21·182	92·283	116·498
$HLCTS_t^{qh}$	47	21·184	92·334	116·544
4 × 4 D				
$HLCTS_r^{qd}$	191	20·357	82·341	111·341
$HLCTS_t^{qd}$	191	20·358	82·374	111·381
$HLCTS_r^{qh}$	191	20·356	82·338	111·341
$HLCTS_t^{qh}$	191	20·358	82·372	111·381
Ref. [30]	–	20·360	–	–

4.2. *Multi-layered spherical shell segments*

This spherical shell segment shown in Figure 4 is doubly curved. It is a nine-layered cross-ply laminate with fibre orientation (0/90/0/90/0/90/0/90/0). It is symmetrically laminated. The side length, a, of the shell segment is 1·0 m (39·37 in). The total thickness of the 0° and 90° layers is the same. The thickness of the laminate is $h = 0{\cdot}01$ m (0·3937 in). The material of the laminate is high modulus graphite/epoxy composite with $E_1/E_2 = 40$, $G_{12}/E_2 = 0{\cdot}6$ and $G_{13}/E_2 = G_{23}/E_2 = 0{\cdot}5$, in which $E_1 = 2{\cdot}0685 \times 10^{11}$ N/m^2 ($3{\cdot}0 \times 10^7$ psi), $\rho = 1605$ kg/m^3 (0·058 lb/in^3) and Poisson's ratio $\nu_{12} = 0{\cdot}25$.

In the first case the shell segment is simply supported at four curved edges. Three finite element meshes: 2 × 2 D, 3 × 3 D and 4 × 4 D are considered for one quarter of the shell. The shear correction factors are $\kappa_4 = \kappa_5 = (5/6)^{1/2}$. The boundary conditions are: $V = \Theta_x = \Theta_z = 0{\cdot}0$ at symmetry line AB, $V = W = \Theta_x = 0{\cdot}0$ at curve edge BC, $U = W = \Theta_y = 0{\cdot}0$ at curve edge CD and $U = \Theta_y = \Theta_z = 0{\cdot}0$ at symmetry line AD. For

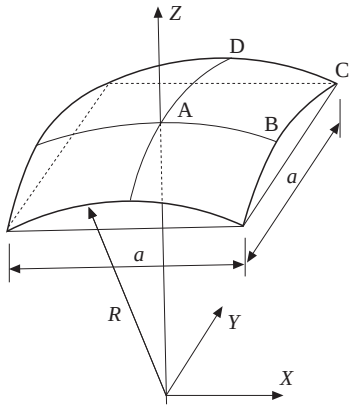

Figure 4. The double curvature spherical shell segment.

TABLE 9

First three dimensionless natural frequencies for the doubly symmetric modes of the simply supported nine-layered cross-ply spherical shell segment

Source	Neq.	Mode sequence 1	2	3
2 × 2 D				
$HLCTS_r^{qd}$	47	0·2473	1·3010	1·4165
$HLCTS_t^{qd}$	47	0·2473	1·3016	1·4170
$HLCTS_r^{qh}$	47	0·2473	1·3010	1·4164
$HLCTS_t^{qh}$	47	0·2473	1·3015	1·4170
3 × 3 D				
$HLCTS_r^{qd}$	107	0·2428	1·2247	1·2866
$HLCTS_t^{qd}$	107	0·2429	1·2251	1·2871
$HLCTS_r^{qh}$	107	0·2428	1·2246	1·2866
$HLCTS_t^{qh}$	107	0·2429	1·2251	1·2871
4 × 4 D				
$HLCTS_r^{qd}$	191	0·2420	1·1281	1·2750
$HLCTS_t^{qd}$	191	0·2420	1·1285	1·2755
$HLCTS_r^{qh}$	191	0·2420	1·1281	1·2750
$HLCTS_t^{qh}$	191	0·2420	1·1285	1·2755
Ref. [23]	–	0·2411	1·063	1·292

the four corners of the finite element model ABCD, all dof are constrained except W at point A, the centre of the shell segment. The displacement and rotation, U and Θ_y, are free at point B. All dof are constrained at C while V and Θ_x are free at point D. Note that these boundary conditions are for doubly symmetrical modes. The HLCTS element results are given in Table 9. The numerical values in the table are dimensionless frequency parameters which are defined in equation (11) with b replaced by h. The analytical solutions for the first three doubly symmetrical modes in the table are from reference [23] in which shear deformation was considered. For the 4 × 4 D mesh, the first mode results applying the HLCTS elements with quadratic polynomial for w converged at the same value 0·2420 which differs from the analytical solution by 0·37%. When using the coarse mesh, 2 × 2 D, the discrepancy is about 2·57%. The latter indicates that the elements proposed in this paper are very efficient as there are only 47 active dof for this 2 × 2 D mesh model. For the higher modes, refined meshes are required for more accurate results.

A comparison with other finite elements is shown in Table 10. The elements include ST6, SQ8, SQ9, SQ11, ST10, SQ12 and SQH. Their properties and characteristics have been described in Table 3 except that now the dof of these elements are, respectively, 30, 40, 45, 55, 50, 60 and 80. For brevity, only the first and second doubly symmetric natural frequencies expressed in the dimensionless frequency parameter defined by equation (10) in which b is replaced by h, are given in Table 10. Since the other HLCTS element results for this problem are presented in Table 9 only the results of $HLCTS_r^{qd}$ are included in Table 10. Also, the SQ4 results are much different from the analytical solutions and are not included here. With reference to Table 10 the overall performances and efficiency of the $HLCTS_r^{qd}$ element is the best.

In the second case, the shell segment in Figure 4 is fully clamped. The non-dimensionalized frequency parameters are included in Table 11. All the geometrical and material properties remain the same as the simply supported case above. It may be

TABLE 10

Comparison of convergence on the dimensionless natural frequency of the nine-layered cross-ply S4 *spherical shell segment by using different finite elements*

Source	Mesh (quarter shell) 2 × 2	3 × 3	4 × 4
First doubly symmetric mode			
ST6	0·2538	0·2459	–
SQ8	0·2452	0·2422	0·2416
SQ9	0·2433	0·2422	–
SQ11	0·2428	–	–
ST10	0·2417	–	–
SQ12	0·2419	–	–
SQH	0·2412	–	–
$HLCTS_r^{qd}$	0·2473	0·2428	0·2420
Analytical [23]		0·2411	
Second doubly symmetric mode			
ST6	1·350	1·173	–
SQ8	1·303	1·136	1·094
SQ9	1·265	1·134	–
SQ11	1·182	–	–
ST10	1·094	–	–
SQ12	1·099	–	–
SQH	1·084	–	–
$HLCTS_r^{qd}$	1·301	1·225	1·128
Analytical [23]		1·063	

noted that in the present case there is no analytical or numerical solution available for comparison.

5. CONCLUDING REMARKS

In this note the consistent mass matrices for the hybrid strain based laminated composite triangular shell (HLCTS) elements have been developed. The following points should be mentioned.

TABLE 11

First three dimensionless natural frequencies for the doubly symmetric modes of the fully clamped nine-layered cross-ply spherical shell segment

Source	Neq.	Mode sequence 1	2	3
4 × 4 D				
$HLCTS_r^{qd}$	169	0·6741	1·5775	1·7393
$HLCTS_t^{qd}$	169	0·6742	1·5781	1·7399
$HLCTS_r^{qh}$	169	0·6741	1·5775	1·7393
$HLCTS_t^{qh}$	169	0·6741	1·5781	1·7399

(1) Together with the element stiffness matrices developed in references [25, 26], the HLCTS elements are all in explicit expressions. There is no numerical matrix inversion and numerical integration involved in the derivations of element matrices.

(2) The HLCTS elements have been applied to solve free vibration problems of single layer and multilayer plates and shells, and only results of some representative multilayer plates and shells are included in this note for brevity. These elements show excellent performance. The comparisons made to the analytical solutions and numerical results obtained by using other finite elements proved that the HLCTS elements are more accurate and efficient than other lower order elements and even comparable to some higher order elements (see Tables 2, 3 and 10). Note that in the vibration analysis higher mode natural frequencies and mode shapes were obtained but not included here for brevity.

(3) There is no shear locking phenomenon detected. The hybrid strain formulation seems to be effective in eliminating shear locking which is problematic in lower order finite elements employing displacement formulation.

(4) The numerical study confirms that the HLCTS elements with a quadratic displacement field for w are more accurate and converge faster than those with a linear field. Whether the moment of inertia is included or not it seems to have no significant effect on results of thin plate and shell structures.

(5) The improved formulation of ddof has eliminated the zero energy modes or spurious modes from the HLCTS elements. With the displacement formulation of ddof, all three zero energy modes are eliminated from the HLCTS elements while the hybrid formulation eliminates one.

(6) Finally, the HLCTS^{qd} and HLCTS^{ld} elements have been found to be the most favourite ones and they are rank sufficient. Because of its ability to give (a) correct number of rigid body modes, and (b) accurate and rank sufficient results, the HLCTS_r^{qd} has further been developed for geometrically non-linear analysis of laminated composite shell structures. The results of this part of the investigation are published elsewhere.

ACKNOWLEDGMENT

The first author gratefully acknowledges the financial support in the form of a research grant from the Natural Sciences and Engineering Research Council of Canada. The investigation was performed while the authors were at the Department of Mechanical Engineering, The University of Western Ontario, London, Ontario, Canada.

REFERENCES

1. C. W. Bert 1985 *Shock and Vibration Digest* **17**(11), 3–25. Research on dynamic behaviour of composite and sandwich plates—IV.
2. C. W. Bert 1987 *Composite Structures* 4, *Proceedings of the Fourth International Conference on Composites and Structures* (I. H. Marshall, editor), **2**, 2.1–2.17. Recent advances in dynamics of composite structures.
3. C. W. Bert 1991 *Shock and Vibration Digest* **23**(6), 3–14. Research on dynamic behaviour of composite and sandwich plates—V: Part I.
4. C. W. Bert 1981 *Shock and Vibration Digest* **23**(7), 9–21. Research on dynamic behaviour of composite and sandwich plates—V: Part II.
5. R. K. Kapania and S. Raciti 1987 *Design and Analysis of Composite Material Vessels* (D. Hui and T. J. Kozik, editors), American Society of Mechanical Engineers, New York, PVP-**121**, 43–54. Recent advances in vibrating and buckling of laminated beams and plates.
6. R. K. Kapania and S. Raciti 1989 *American Institute of Aeronautics and Astronautics Journal* **27**, 935–946. Recent advances in analysis of laminated beams and plates, Part II: vibration and wave propagation.
7. J. G. Ren 1990 *Handbook of Ceramics and Composites* (N. P. Cheremisinoff, editor) **1**, 413–450. Bending, vibration and buckling of laminated plates.

8. J. N. Reddy 1985 *Shock and Vibration Digest* **17**(4), 3–8. A review of the literature on finite element modelling of laminated composite plates.
9. J. N. Reddy 1990 *Shock and Vibration Digest* **22**(7), 3–17. A review of refined theories of laminated composite plates.
10. R. K. Kapania 1989 *Journal of Pressure Vessel Technology* **111**, 88–96. A review on the analysis of laminated shells.
11. H. T. Y. Yang, S. Saigal and D. G. Liaw 1990 *Computers and Structures* **35**, 481–504. Advances of thin shell finite elements and some applications—version I.
12. A. K. Noor and W. S. Burton 1990 *Applied Mechanics Review* **43**, 67–96. Assessment of computational models for multilayered composite shells.
13. K. Kamal and S. Durvasula 1986 *Computers and Structures* **5**, 177–202. Some studies of free vibration of composite laminates.
14. T. J. Craig and D. J. Dawe 1986 *International Journal of Solids and Structures* **22**, 155–169. Flexural vibration of symmetrically laminated composite rectangular plates including transverse shear effects.
15. R. L. Ramkumar, P. C. Chen and W. J. Sanders 1987 *American Institute of Aeronautics and Astronautics Journal* **25**, 146–151. Free vibration solution for clamped orthotropic plates using Lagrangian multiplier technique.
16. J. A. Bowlus, A. N. Palazotto and J. M. Whitney 1987 *American Institute of Aeronautics and Astronautics Journal* **25**, 1500–1511. Vibration of symmetrically laminated rectangular plates considering deformation and rotatory inertia.
17. A. A. Khdeir 1988 *Journal of Sound and Vibration* **122**, 377–388. Free vibration of antisymmetric angle-ply laminated plates including various boundary conditions.
18. A. T. Chen and T. Y. Yang 1988 *Journal of Composite Materials* **22**, 341–359. A 36 DOF symmetrically laminated triangular element with shear deformation and rotatory inertia.
19. H. P. Huttelmaier and M. Epstein 1989 *Journal of Engineering Mechanics* **115**, 315–325. Multi-layered finite element formulation for vibration and stability analysis of plates.
20. P. Lardeur and J. L. Batoz 1989 *International Journal for Numerical Methods in Engineering* **27**, 343–359. Composite plate analysis using a new discrete shear triangular finite element.
21. R. R. Kumar and Y. V. K. S. Rao 1988 *Computers and Structures* **28**, 717–722. Free vibrations of multilayered thick composite shells.
22. A. K. Noor and J. M. Peters 1989 *Journal of Engineering Mechanics* **115**(6), 1225–1244. A posteriori estimates for shear correction factors in multilayered composite cylinders.
23. A. K. Noor and M. D. Mathers 1975 *NASA TN D*-8044, Washington, D.C. Shear-flexible finite element models of laminated composite plates and shells.
24. A. K. Noor and W. S. Burton 1989 *Applied Mechanics Review* **42**, 1–12. Assessment of shear deformation theories for multilayered composite plates.
25. C. W. S. To and B. Wang 1995 *Proceedings of the* 15*th Canadian Congress of Applied Mechanics*, May 28–June 1, University of Victoria, B.C., Canada **1**, 226–227. Analysis of laminated composite shell structures by hybrid strain based laminated flat triangular elements.
26. C. W. S. To and B. Wang 1998 *Finite Elements in Analysis and Design* **28,** 177–207. Hybrid strain based three-node flat triangular laminated composite shell elements.
27. M. L. Liu and C. W. S. To 1995 *Journal of Sound and Vibration* **184**(5), 801–821. Vibration of structures by hybrid strain based three-node flat triangular shell elements.
28. J. N. Reddy and N. D. Phan 1985 *Journal of Sound and Vibration* **98**, 157–170. Stability and vibration of isotropic, orthotropic and laminated plates according to a high order shear deformation theory.
29. K. P. Soldatos 1987 *Journal of Sound and Vibration* **119**, 111–137. Influence of thickness shear deformation on free vibrations of rectangular plates, cylindrical panels and cylinders of antisymmetric angle-ply construction.
30. J. N. Reddy and C. F. Liu 1985 *International Journal of Engineering Science* **23**, 319–330. A higher-order shear deformation theory of laminated elastic shells.